NOTATION

q, heat flux, W/m^2; ΔT, temperature differential, °K; α, heat-transfer coefficient, $W/m^2 \cdot °K$; P, pressure, N/m^2; P_{cr}, critical pressure, N/m^2; P_*, reference pressure, N/m^2; n, a power exponent; C, a proportionality factor; Φ, F_1, special functions.

LITERATURE CITED

1. R. D. Cummings and J. L. Smith, in: Liquid Helium Technology (Suppl. Bull. I.I.F./I.I.R. Annexe 1966-5), Int. Inst. Refrigeration, Paris (1966), pp. 85-95.
2. L. Bewilogua, R. Knöner, and H. Vinzelberg, Cryogenics, 15, No. 3, 121-125 (1975).
3. D. N. Lyon, Int. Adv. Cryog. Eng., 10, Part 2, 371-379 (1965).
4. V. M. Borishanskii, in: Topics in Heat Transfer and Hydraulics of Two-Phase Media [in Russian], Gosénergoizdat, Moscow-Leningrad (1961), p. 18.

INVESTIGATION OF THE EVAPORATION PROCESS AND SONIC LIMITS IN SODIUM HEAT PIPES

M. N. Ivanovskii, V. V. Prosvetov, V. P. Sorokin, B. A. Chulkov, and I. V. Yagodkin

UDC 669.536.422

The maximum heat fluxes in the heating zone and the sonic limits of power transfer in sodium heat pipes and vapor chambers with composite (channel) wicks are investigated experimentally.

Heat pipes with composite wicks [1] are attractive for the rather unique possibilities that they afford for heat transfer and operation in various positions relative to the field of gravity. However, they have a substantial drawback: Their capillary hysteresis effect is such that even the slightest drying of the wick is enough to drastically reduce heat transfer. It is especially important, therefore, to know the limiting characteristics of such heat pipes and to ascertain all the processes that can lead to dryout of composite wicks.

Specific Heat Fluxes. We have conducted investigations of these effects in the heating zone in a sodium vapor chamber. The working surface to be heated by condensed sodium vapor had a diameter of 24 mm and a thickness of 0.3 mm; it was formed on a flat vertical heat-resistant steel wall. It was equipped with a composite wick, whose perforated screen was situated at a distance of 0.45 mm from the wall. A screen having a small surface porosity $\varepsilon = 0.08$ was used in order to attain high specific heat fluxes on the evaporation mirror. The holes in the screen had a diameter of 0.15 mm and were arrayed in a staggered pattern with a spacing of 0.5 mm. We measured the temperature of the heated wall, the vapor temperature in the vapor chamber, and the heating and flow of water transporting heat from the vapor chamber. Typical data from these experiments are summarized in Table 1.

At low vapor pressures the specific heat fluxes are limited by kinetic evaporation. The maximum heat flux for evaporation in vacuum can be represented by the expression

$$(q_0)_{max} = f \frac{L_0 P_0}{\sqrt{2\pi R T_0/\mu}}. \quad (1)$$

If, on the other hand, the vapor has pressure P_V and the corresponding saturation temperature T_V, the following relation can be used for the heat flux in evaporation [2]:

$$q_0 = f\varkappa \left[\frac{L_0 P_0}{\sqrt{2\pi R T_0/\mu}} - \frac{L_V P_V}{\sqrt{2\pi R T_V/\mu}} \right], \quad (2)$$

Translated from Inzhenerno-Fizicheskii Zhurnal, Vol. 33, No. 5, pp. 832-837, November, 1977. Original article submitted November 22, 1976.

0022-0841/77/3305-1306$07.50

where

$$\varkappa = \frac{1/f}{1/f - 1/2 + v/4c}; \quad c = \sqrt{\frac{8RT_v}{\pi\mu}}.$$

The evaporation coefficient is close to unity for liquid metals having a clean surface. An accumulation of contaminants on the unrenewed surface can cause a reduction in f. In evaporation tests, for example, Knudsen [3] observed a decrease in the evaporation coefficient to a value of order 10^{-3} for mercury. Although one should not expect such strong effects due to contaminants for alkali metals as for mercury, certainly the degree of influence can be estimated in the experiments. The calculation of f according to expression (2) for the experimental data shows that the evaporation coefficient is close to unity.

The vapor chamber was flushed twice with sodium condensate prior to the experiments. The data given above were obtained after 20 h of operation in the evaporation regime with large heat fluxes. Dryout of the composite wick was observed in the sodium vapor chamber experiments. Calculations show that the total vapor–liquid pressure difference in this regime is close to the available capillary head and that the greatest contribution is from the pressure difference at the phase transition.

Sonic Limits. We have conducted an experimental study of the sonic (gasdynamic-choking) limits of power transfer in two modifications of horizontal sodium heat pipes differing in their geometric dimensions. The first heat pipe had a vapor-channel 14 mm in diameter, a heating length of 100 mm, an adiabatic section 50 mm long, and a condenser section 550 mm long. The screen of the composite wick was a thin-walled tube perforated with a staggered array of holes 0.45 mm in diameter in the heating zone. The surface porosity of the screen was 33%. The space between the body of the pipe and the screen was 0.5 mm.

The second heat pipe had a vapor-channel diameter of 12 mm and was heated over a length of 400 mm. The adiabatic and condenser had respective lengths of 150 and 450 mm. The screen of the composite wick comprised fine-mesh porous tubes. The effective pore radius was 0.013 mm, and the space for passage of the liquid was 0.23 mm.

The heat pipes were heated by condensed sodium vapor. Cooling was effected by water through a gas-filled buffer space with a regulated thermal resistance. The temperature along the length of the vapor space of the heat pipes was measured with a movable thermocouple, which was moved in a case 1 mm in diameter. The results of our experimentals for heat-transfer values up to 8 kW/cm^2 are given in Fig. 1.

The sonic limit of power transfer in heat pipes has been investigated in several theoretical and experimental papers, for example [4-6]. The disparities between the results of calculations according to the relations given in those papers is sizable. The simplest hydrodynamic model on which the indicated relations are based is the ideal mass-injection nozzle. The latter is characterized by isentropic gas flow. What this means in application to the heat pipe is that the vapor entering the main flow must have the same characteristics as the main flow.

An analytical model based on an isenthalpic mass-injection nozzle (Levy [5]) is more consistent with the vapor-flow conditions in heat pipes. However, Levy [5] ignores the effect of friction on the sonic limit and postulates a discontinuous (shock) velocity profile.

TABLE 1. Specific Heat Fluxes in Evaporation

Experimental point	1	2*	3
Wall temperature T_W, °C	685	700	730
Evaporation surface temperature† T_0, °C	645	655	700
Vapor temperature at evaporation surface‡ T_V, °C	550	565	655
Vapor temperature in vapor chamber T_V, °C	610	620	670
Heat flux at wall q_W, W/cm^2	345	390	235
Heat flux at evaporation surface q_0, W/cm^2	2100	2500	2750

*Regime preceded by dryout.

† Temperature calculated with allowance for crowding of heat-flux lines at pore surfaces (numerical solution).

‡ Temperature calculated with allowance for pressure recovery during outflow of vapor from wick pores.

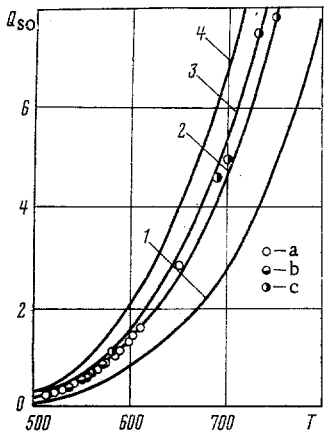

Fig. 1

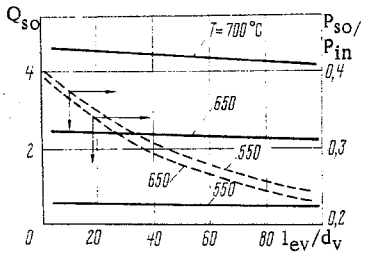

Fig. 2

Fig. 1. Comparison of calculated and experimental values of the sonic limit Q_{so}, kW/cm^2, versus temperature T, °C, in sodium heat pipes. 1) Isentropic thick-walled nozzle model [6]; 2) authors' calculation for isenthalpic mass-injection nozzle model with friction; 3) isenthalpic mass-injection nozzle without friction [5]; 4) isentropic mass-injection nozzle model; a) experimental data of Kemme [4]; b) heat pipe No. 1; c) No. 2.

Fig. 2. Variation of the sonic limit of power transfer Q_{so}, kW/cm^2, and the ratio of the vapor pressure in the critical cross section to the pressure at entry to the evaporation section P_{so}/P_{in} versus length of the evaporator section.

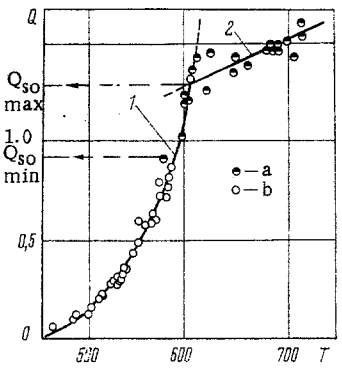

Fig. 3

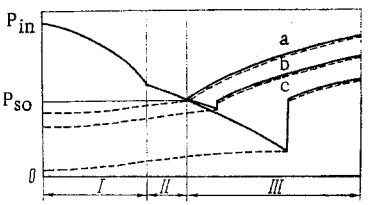

Fig. 4

Fig. 3. Power limitations in experiments on heat pipe No. 3. a) Dryout of heat pipe; b) no dryout; 1) sonic limit; 2) capillary limit curve fitted to the experimental points.

Fig. 4. Pressure variation of vapor (solid curves) and liquid (dashed curves) along heat pipe in sonic regime as a function of cooling rate of condenser section. The cooling rate increases from a to c. I) Evaporator section; II) adiabatic section; III) condenser section.

To describe the hydrodynamics of the vapor in heat pipes we use the one-dimensional energy equation for variable-mass flow; for a pipe of constant cross section it has the form [7]

$$\frac{d\rho}{\rho} + \beta W dW + W^2 d\beta + \rho W^2 \frac{dG}{G} + \xi \frac{W^2}{2} \frac{dx}{d_v} = 0. \qquad (3)$$

The lengthwise momentum-flux coefficient β along the evaporator and adiabatic sections is calculated by numerical integration of the velocity profile over the pipe cross section. The velocity profile in the evaporator section is specified as a function of the local values of the Reynolds axial-flow and crossflow Reynolds numbers according to equations derived by Busse [8]. In the adiabatic zone we assume the velocity profile of stabilized constant-mass flow. We assume that the friction coefficient in the first approximation depends only on the axial Reynolds number without regard for distortion of the velocity profile by evaporation. Under this assumption

the influence of friction in the evaporator section is only slightly overestimated for short evaporator sections, i.e., such that the overall influence of friction is small. The errors incurred by the given assumption can be appreciable for long evaporator sections. The energy-flux equation (3) is augmented with the equation of continuity and the equation of state of the vapor.

We integrated the system of equations numerically on a computer. The initial conditions were specified at the end of the heat pipe. The parameters of the vapor along the length of the pipe were calculated with allowance for flow compressibility on the assumption of an equilibrium state at the saturation line. The integration was carried out by an iterative procedure until the Mach number M attained a value of unity at the entrance to the condenser section.

The results of numerical integration according to the program written for the problem are given in Fig. 1. A comparison with our experimental data and with those of Kemme [4] shows that the computational results are in good agreement with experiment. The model of a frictionless isenthalpic mass-injection nozzle [5] yields acceptable results for heat pipes with comparatively short evaporator and adiabatic sections. The isentropic mass-injection nozzle model gives excessive results.

Figure 2 illustrates the influence of friction on the sonic limits as a function of the length of the evaporator section according to our computations. Up to relatively large evaporator lengths ($l_{ev}/d_v \simeq 100$), the influence of friction is small, not more than 15%. Its influence in the adiabatic section is also inconsequential.

It was observed in the sodium heat pipe experiments that dryout of the wick due to capillary limits can occur in sonic regimes, extending to part of the sonic-limit curve.

The results of measurements of the peak power output of a sodium heat pipe operating in the horizontal position are given in Fig. 3. A pipe 960 mm in length with a vapor channel 11 mm in diameter was heated over a length of 400 mm. The wick was a porous tube consisting of three layers of serge mesh with surface pores 48 μ in diameter. The wick was installed in the body of the pipe with a 0.55-mm space for passage of the liquid. Dryout was obtained by increasing the temperature of the heat pipe with rapid cooling of the condenser section (i.e., moving upward along the sonic limit curve) and by making the transition from the subsonic to the sonic regime with a simultaneous increase in the cooling rate and decrease in the temperature of the heat pipe. The possibility of the capillary limits extending to part of the sonic-limit curve is explained by the fact that the pressure differentials can vary from a maximum value equal to the pressure P_{in} at the entrance to the heating zone to a minimum value $P_{in} - P_{so}$, where P_{so} is the pressure in the critical cross section, depending on the cooling rate for one given value of the transferred power in the sonic regime (Fig. 4). Under the condition that the pressure differentials in the liquid inside the wick are small, the lower bound of the sonic power $(Q_{so})_{min}$ at which capillary limitations set in for the case of rapid cooling can be approximately determined from the relation

$$(Q_{so})_{min}/(Q_{so})_{max} \simeq 1 - P_{so}/P_{in} \qquad (4)$$

in which $(Q_{so})_{max}$ is the power corresponding to the intersection of the curves for the sonic and capillary limits (Fig. 3).

We point out that the ratio P_{so}/P_{in} is not constant; because of friction, it depends on the lengths of the evaporator and adiabatic sections (Fig. 2). For heat pipes with short evaporator and adiabatic sections the ratio $P_{so}/P_{in} = 0.4$, and, accordingly, $(Q_{so})_{min}/(Q_{so})_{max} = 0.6$. For the experiments represented in Fig. 3, according to analytical estimates, we have $(Q_{so})_{min}/(Q_{so})_{max} = 0.75$, which is not inconsistent with the measurement results

The possible inception of capillary limitations in sonic regimes must be taken into account when heat pipes are intended to be used for maximum heat delivery under conditions such that isothermicity of the heat pipe is not significant.

NOTATION

P, vapor pressure; T, temperature; ρ, density; μ, molecular weight; L, latent heat of vaporization; q, specific heat flux in heating zone; Q, specific heat transfer along heat pipe; G, mass flow of vapor in pipe cross section; W, average vapor flow velocity in pipe; ε, surface porosity of wick; R, universal gas constant; f, coefficient of evaporation; β, momentum-flux coefficient; ξ, coefficient of friction; d_v, diameter of heat pipe vapor channel. Indices: 0, liquid surface; v, vapor at liquid surface; w, wall surface; in, entrance to heating zone; so, critical cross section.

LITERATURE CITED

1. M. N. Ivanovskii, V. P. Sorokin, and V. I. Subbotin, Evaporation and Condensation of Metals [in Russian], Atomizdat, Moscow (1976).
2. R. Risch, Helv. Phys. Acta, 6, 132 (1933).
3. M. Knudsen, Ann. Phys. (Leipzig), 47, 697 (1915).
4. I. E. Kemme, "Heat pipe capability experiments," in: The IEEE Thermionic Conversion Specialist Conference, Houston, Texas, LA-3585 (1966).
5. E. K. Levy, "Theoretical investigation of heat pipes operating at low vapor pressures," Trans. ASME, Ser. B: J. Eng. Ind., 90, 547 (1968).
6. H. W. H. van Andel, "Heat pipe design theory," in: the International Conference on Thermionic Electrical Power Generation, Paper D-5, Stresa (1968).
7. L. A. Vulis, Thermodynamics of Gas Flows [in Russian], Izd. Gos. Énerg., Moscow-Leningrad (1950).
8. C. A. Busse, "Pressure drop in the vapor phase of long heat pipes," in: Thermionic Conversion Specialist Conference, Palo Alto, California (1967).